S & M 4242

# Design and Performance Evaluation of Circuit Architectures and Placement Strategies for Insole-based Piezoelectric Energy Harvesting under Human Gait

Shang-Kuo Yang, Po-Yang Shih, and Kai-Jung Chen\*

Department of Mechanical Engineering, National Chin Yi University of Technology, Taichung 41170, Taiwan, R.O.C.

(Received September 5, 2025; accepted November 19, 2025)

*Keywords:* piezoelectric energy harvesting, wearable electronics, gait analysis, DC parallel circuit, battery charging

Wearable piezoelectric energy harvesting offers a promising solution for powering low-power sensing modules in self-sustained health monitoring systems. In this study, we present an insole-integrated piezoelectric energy harvesting framework and experimentally evaluate the effects of transducer placement and circuit configuration under realistic gait conditions. The results reveal that DC parallel rectification provides consistently superior charging capability, whereas the EH301A energy management module enhances output stability through automated regulation. These findings establish circuit selection criteria for intermittent biomechanical excitation and highlight the feasibility of self-powered insole sensors for IoT-based wearable applications. The proposed system functions as a self-powered insole sensor that simultaneously detects plantar-pressure-induced strain and converts it into regulated electrical energy for wearable electronics, demonstrating sensing-enabled energy harvesting relevance to Smart Footwear and IoT-based health monitoring applications.

#### 1. Introduction

The global transition toward sustainable energy systems has highlighted the urgent need for decentralized power solutions capable of supporting the growing number of portable and wearable electronic devices. While renewable sources such as solar, wind, and hydropower have demonstrated large-scale effectiveness, their dependence on specific environmental or geographic conditions limits their applicability for small, mobile systems. In contrast, the biomechanical energy generated during human locomotion is continuous, widely available, and independent of environmental constraints, making it an attractive candidate for wearable applications such as self-powered sensors and health-monitoring devices.<sup>(1–3)</sup>

Piezoelectric energy harvesting has emerged as a particularly promising approach owing to its ability to directly convert mechanical strain into electrical energy with relatively high energy density. Prior research has explored piezoelectric tiles in public spaces, producing up to hundreds

\*Corresponding author: e-mail: <a href="https://doi.org/10.18494/SAM5926">https://doi.org/10.18494/SAM5926</a>

of watts per day in high-footfall environments.<sup>(4,5)</sup> More recently, the integration of piezoelectric ceramics into footwear has been investigated, leveraging the repetitive high-pressure peaks occurring at the heel and forefoot during the gait cycle.<sup>(6–8)</sup> These regions consistently experience ground reaction forces exceeding body weight, providing localized and repeatable inputs for energy conversion.

Despite these advancements, critical gaps remain in the current literature. Many existing footwear-based studies mainly report voltage increments and do not quantify current, power, or harvested energy, which are necessary to evaluate charging capability. Although different circuit topologies have been introduced, few studies have compared their performance under realistic gait conditions. In addition, the optimization of placement or circuit design is often mentioned without a clear or systematic methodology. These shortcomings reduce the academic rigor of the field and hinder the translation of experimental results into practical, safe, and scalable applications.<sup>(9–11)</sup>

The objective of this study is to address these deficiencies by presenting the design, optimization, and experimental evaluation of a shoe-insole piezoelectric energy harvesting and charging system. Two PZT-5 ceramic plates were embedded in the heel and metatarsal regions, identified as optimal on the basis of plantar pressure distribution analysis. Multiple circuit architectures—including AC and DC series/parallel arrangements as well as a commercial energy management module—were implemented and tested under treadmill walking at different speeds. Unlike previous studies, the evaluation extends beyond battery voltage rise to include comprehensive energy metrics (voltage, current, power, and energy in mWh).

This work contributes to the advancement of wearable energy harvesting by (i) clarifying the effects of piezoelectric plate placement and circuit topology on energy efficiency, (ii) identifying the DC parallel configuration as the most reliable solution under gait-induced asynchronous loading, and (iii) providing practical insights for integrating such systems into self-powered wearable sensors and smart footwear platforms. In practical wearable environments, the electrical performance of piezoelectric energy harvesters is governed by four primary factors: (i) the magnitude and distribution of plantar pressure, which determines the induced strain in the piezoelectric material; (ii) the intrinsic piezoelectric coefficient and mechanical robustness of the transducer; (iii) the impedance matching and rectification strategy of the circuit, which directly affect power transfer efficiency; and (iv) the timing characteristics of heel-strike and toe-off events, where asynchronous excitation may lead to partial cancellation if suboptimal circuit design is used. These factors collectively control the amount of electrical charge generated per gait cycle and must be optimized simultaneously for practical power generation in wearable devices. These findings not only fill existing gaps in the academic literature but also pave the way for scalable applications in health monitoring, mobile electronics, and IoT.

#### 2. Materials and Methods

#### 2.1 Overview of experimental design

This study was designed to evaluate the performance of a shoe-insole piezoelectric energyharvesting system intended for powering wearable sensors. The experimental framework involved embedding piezoelectric ceramic plates in key plantar regions identified from gait biomechanics and coupling them with different circuit configurations. The system was assessed under controlled treadmill walking conditions at three speeds (3, 4, and 5 km/h) for 1 h trials.

The core objectives were as follows.

- (1) To compare the effectiveness of different circuit architectures (AC vs DC, series vs parallel, and a commercial energy management module)
- (2) To investigate the effect of piezoelectric output voltage on the charging behavior of a lithiumion battery under different walking speeds
- (3) To determine the optimal piezoelectric plate placement and circuit topology for practical wearable applications

Figure 1 illustrates the overall experimental framework, showing the conversion of gait-induced vibration energy into electrical voltage through piezoelectric transducers, rectification, and its subsequent effect on battery charging.

#### 2.2 Materials

The piezoelectric energy harvesting system consisted of insole-embedded piezoelectric plates, rectifier circuits, and energy storage components. The material selection was guided by three principles: (i) ensuring sufficient energy conversion efficiency under cyclic biomechanical loading, (ii) enabling a safe and stable charging of a lithium-ion battery, and (iii) providing a reliable measurement of voltage to allow a reproducible evaluation of charging behavior.

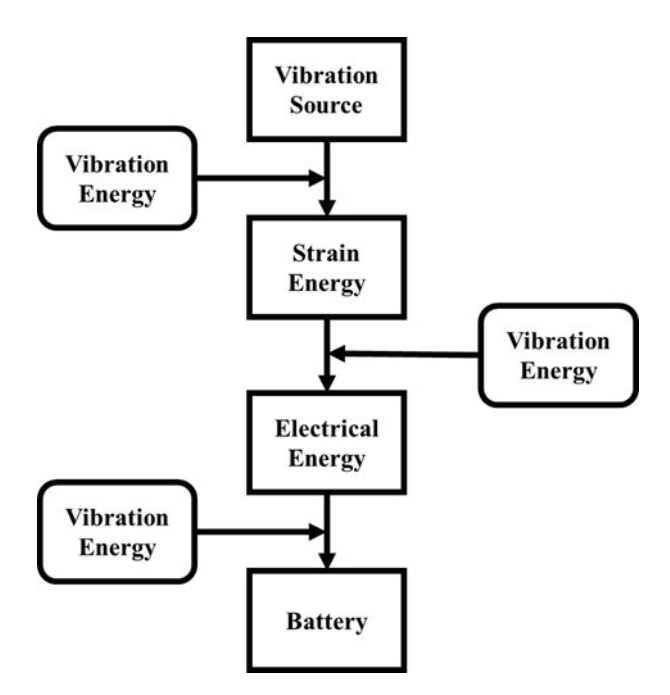


Fig. 1. Schematic diagram of the piezoelectric energy conversion process and battery charging framework.

#### 2.2.1 Piezoelectric elements

Two lead zirconate titanate (PZT-5) ceramic plates, supplied by Superex Technology Co., Ltd., were used as the main energy transducers. The first plate (Plate A) measured  $60 \times 20 \times 0.8$  mm with a free length of 53 mm and total deflection > 2.5 mm, whereas the second plate (Plate B) measured  $40 \times 20 \times 0.8$  mm with a free length of 33 mm and total deflection > 1.5 mm shown in Fig. 2. The PZT-5 ceramic, as shown in Fig. 3, with a piezoelectric coefficient of approximately d33  $\approx$  390 pC/N, was selected owing to its high energy density and acceptable robustness compared with polymer-based alternatives. The two plates were embedded under the heel and metatarsal regions of the insole, guided by plantar pressure distribution. Figure 4 illustrates the principle of piezoelectric transduction, in which applied mechanical stress induces electrical polarization and charge generation. Moreover, the specifications of two PZT-5 ceramics are described in Table 1.

#### 2.2.2 Insole material

The insole was fabricated using *UdiLife natural latex* (28 cm in length shown in Figure 5), chosen for its softness and mechanical adaptability, ensuring tight coupling between the PZT plates and the plantar surface. This provided efficient mechanical-to-electrical energy transfer and improved durability under repeated loading.



Fig. 2. (Color online) Placement of piezoelectric plates in the insole.

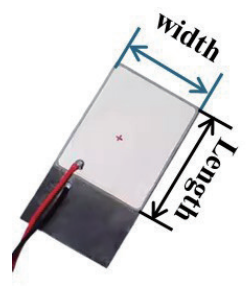


Fig. 3. (Color online) PZT-5 ceramic plates.

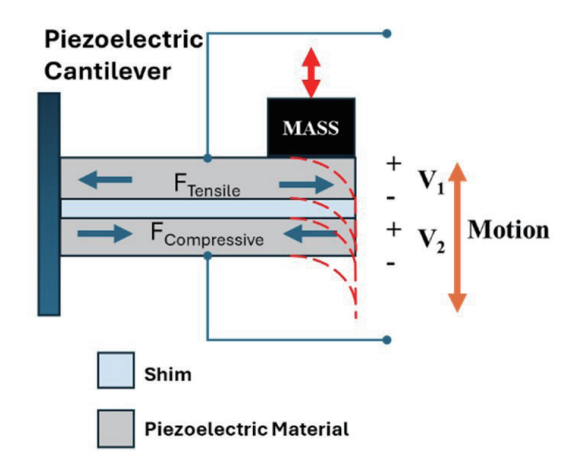


Fig. 4. (Color online) Schematic diagram of piezoelectric transduction principle.

Table 1 Specifications of PZT-5 plates: Plates A and B.

PZT-5 ceramic piezoelectric plates	A. Large size specifications	B. Small size specifications
Length	60 mm	40 mm
Width	20 mm	20 mm
Thickness	0.8 mm	0.8 mm
Free length	53 mm	33 mm
Maximum deflection	>2.5 mm	>1.5 mm
Piezoelectric coefficient (d33)	~390 pC/N (approx.)	~390 pC/N (approx.)



Fig. 5. (Color online) UdiLife natural latex insole.

# 2.2.3 Energy storage components

The harvested energy was directed to a Nokia BL-5B lithium-ion battery (3.7 V, 890 mAh) as the primary storage unit. To support comparative evaluation, a test capacitor (1000  $\mu$ F, 16 V) was also included to capture transient charging behavior shown in Figure 6 and Table 2. The capacitor enabled the observation of immediate voltage increments under cyclic loading, whereas the battery allowed the evaluation of long-term charging feasibility.



Fig. 6. (Color online) Nokia BL-5B lithium ion battery.

Table 2 Specifications of energy storage components.

Component	Specification	Notes
Battery	Nokia BL-5B, 3.7 V, 890 mAh and end charge voltage: 4,2V	Rechargeable lithium-ion battery
Capacitor	1000 μF, 16 V	Used for transient charge-discharge analysis

# 2.2.4 Circuit components

The piezoelectric energy harvesting system was constructed using a three-part architecture: (1) piezoelectric transducers that generate AC voltage under mechanical loading, (2) rectifier circuits that convert AC to DC, and (3) energy storage units for accumulating the harvested energy.

Figure 7 illustrates the complete schematic. The left section represents the equivalent circuit model of a piezoelectric plate, modeled as an AC voltage source with an intrinsic capacitance and leakage resistance in parallel. This configuration effectively captures the dynamic charge generation and storage behavior of PZT ceramics under cyclic gait-induced stress. The right section of Fig. 7 shows the rectifier and storage stage. A full-bridge rectifier constructed from four fast-switching Schottky diodes was used to minimize forward voltage drop, followed by a smoothing capacitor to suppress voltage ripple and stabilize the DC output. The rectified energy was directed to a rechargeable Nokia BL-5B lithium-ion battery (3.7 V, 890 mAh).

To systematically evaluate circuit performance, four rectifier topologies were implemented (Fig. 8): (a) AC series, (b) AC parallel, (c) DC series, and (d) DC parallel. These configurations provided a controlled comparison between voltage-maximizing and current-maximizing strategies. In addition, a commercial EH301A power management module (Advanced Linear Devices, Fig. 9) was tested as a benchmark. The commercial EH301A module (Advanced Linear Devices, USA) is a dedicated power management circuit designed for piezoelectric and other high-impedance energy sources. It features an internal storage capacitor and an automatic charge—discharge mechanism based on hysteresis voltage thresholds (VH = 5.2 V, VL = 3.1 V). Once the upper threshold is reached, the stored energy is released to the load in efficient bursts, ensuring regulated output suitable for wearable electronics.

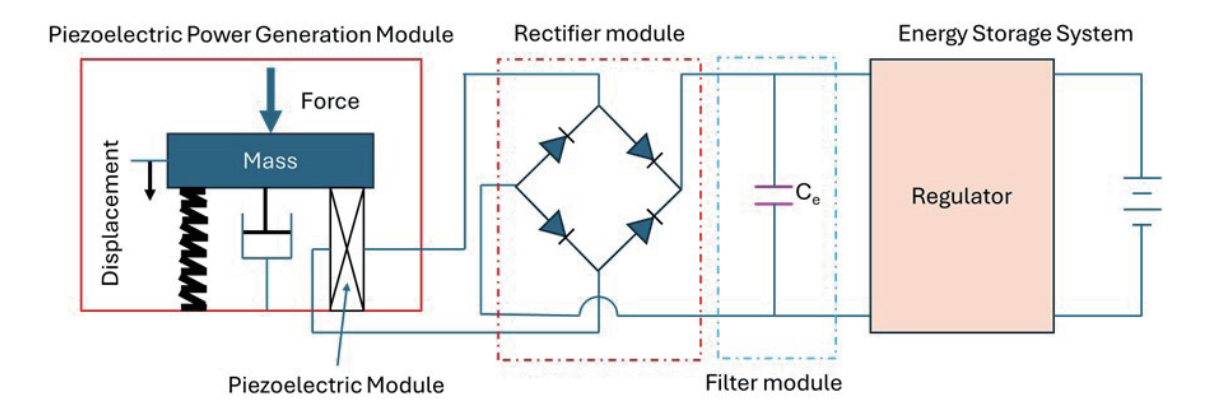


Fig. 7. (Color online) Equivalent circuit model of the piezoelectric harvesting system.

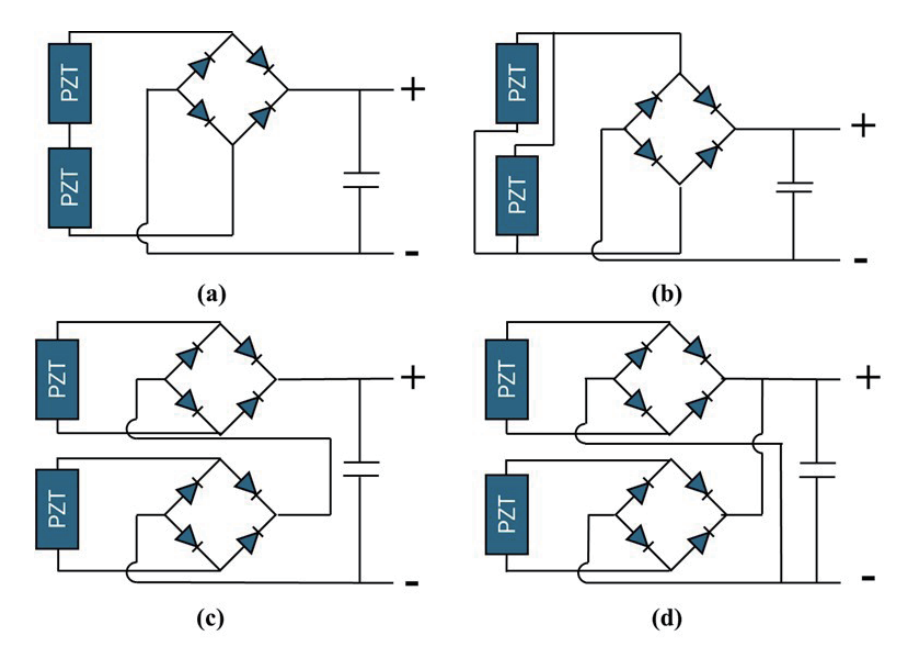


Fig. 8. (Color online) Four bridge rectifier configurations: (a) AC series, (b) AC parallel, (c) DC series, and (d) DC parallel.

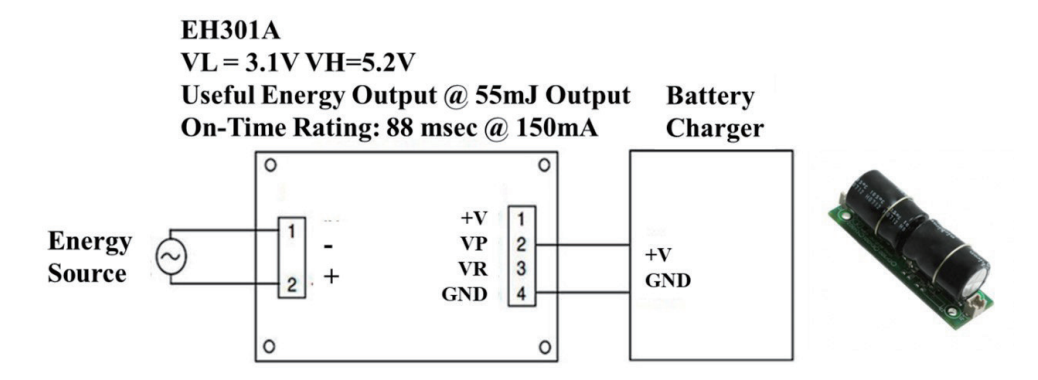


Fig. 9. (Color online) EH301A power management module.

This integrated design enables the irregular AC output generated during gait to be effectively rectified, stabilized, and stored, providing a reliable energy harvesting pathway for wearable electronics.

#### 2.2.5 Measurement instruments

The FLUKE-287 true RMS digital multimeter (Fig. 10) was employed to measure AC and DC voltages generated by the piezoelectric system. Its high-resolution 50000-count display and 0.025% basic DC accuracy ensured the precise tracking of voltage variations during walking trials. The instrument's ability to capture transient voltage changes was particularly important for characterizing the irregular outputs of gait-induced piezoelectric energy harvesting.

In this study, the primary evaluation metrics were the voltage developed across the test capacitor ( $1000 \, \mu F$ ,  $16 \, V$ ) and the incremental voltage rise of the lithium-ion battery (Nokia BL-5B,  $3.7 \, V$ ,  $890 \, \text{mAh}$ ). Capacitor voltage responses were used to assess short-term storage behavior, while battery voltage increments provided a measure of long-term charging feasibility. By combining capacitor-based and battery-based evaluations, this approach allowed the reproducible assessment of the charging effect under different gait conditions without relying solely on open-circuit voltage measurements. A simplified functional pathway of the sensing-driven energy harvesting system is illustrated in Fig. 11. It highlights the conversion of human gait forces into electrical signals, their rectification and conditioning, and the subsequent energy accumulation in storage devices for evaluating charging performance.

## 2.2.6 Functional summary

For clarity, the roles of the major components in the system are summarized as follows. The PZT-5 ceramic plates (Superex) served as transducers, converting gait-induced mechanical stress into alternating voltage. The natural latex insole (UdiLife) ensured mechanical coupling and durability under repeated loading. Rectifier circuits based on Schottky diodes conditioned the AC signals into DC for storage. A 1000  $\mu$ F capacitor was used to enable short-term voltage tracking and transient charge–discharge analysis, while a Nokia BL-5B lithium-ion battery (3.7)



Fig. 10. (Color online) FLUKE-287 handheld digital multimeter.

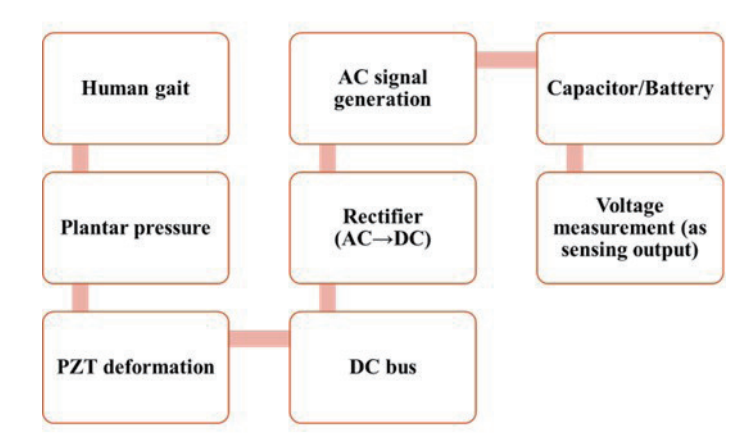


Fig. 11. (Color online) Signal flow pathway of the insole-based piezoelectric sensing and energy harvesting system.

V, 890 mAh) was employed to evaluate long-term charging feasibility. The EH301A commercial module (Advanced Linear Devices) was included as a benchmark for integrated power management. Finally, electrical outputs were characterized using a Fluke 287 multimeter, which provided accurate measurements of voltage to support both capacitor-based evaluation and battery charging assessment.

#### 2.3 Methods

## 2.3.1 Experimental setup

The experimental platform consisted of an insole-embedded piezoelectric energy harvesting system, comprising PZT-5 ceramic plates, rectifier circuits, and energy storage units. Each insole was fabricated from natural latex (UdiLife, 28 cm length), with piezoelectric plates firmly embedded beneath the heel and metatarsal regions to ensure close coupling with plantar pressure. The plates were electrically connected to external rectifier circuits and storage units via flexible leads routed along the side of the insole to minimize discomfort.

The insole system was worn by healthy adult participants (n = 5, aged 18–30 years) during treadmill walking to ensure reproducible loading conditions. All experiments were performed indoors under controlled laboratory conditions (ambient temperature 22–25 °C, humidity 45–55%) to minimize environmental variability. The overall setup was designed to replicate realistic walking while maintaining consistent and repeatable test conditions.

## 2.3.2 Gait simulation and loading conditions

Walking experiments were conducted on a BH G6415T treadmill at controlled speeds ranging from 3 to 5 km/h. This speed range was chosen to represent typical human walking conditions while maintaining consistency across trials. These speeds correspond to common human gait cadences ranging from approximately 95 to 125 steps per min, ensuring

biomechanically realistic heel-strike and push-off loading without inducing abnormal gait patterns or transitioning into jogging dynamics. Participants wore standard lightweight shoes to ensure comparable foot—insole contact across all experiments.

The biomechanical loading during walking was characterized by heel strike, mid-stance, and toe-off phases. Previous studies have shown that these events produce two dominant ground reaction force peaks of approximately  $1.08 \times BW$  and  $1.16 \times BW$ . By embedding the piezoelectric plates under the heel and metatarsal regions, the system was positioned to capture these high-pressure loading events.

Each walking trial lasted between 1 and 10 min, depending on the objective of the measurement. Short trials were used to examine transient charging effects, while longer trials enabled the evaluation of quasi-steady-state behavior. Between trials, participants rested to avoid fatigue, and storage devices (capacitor or battery) were reset to baseline voltage levels to ensure comparability.

## 2.3.3 Circuit testing procedure

Four rectifier circuit configurations were systematically evaluated: (a) AC series, (b) AC parallel, (c) DC series, and (d) DC parallel. Each configuration employed identical piezoelectric plate inputs, ensuring that observed differences in performance were attributable solely to circuit topology. In the AC series and AC parallel arrangements, the two piezoelectric plates were combined before rectification, while in the DC series and DC parallel designs, each plate was individually rectified before being combined.

The commercial EH301A power management module (Advanced Linear Devices) was also tested under the same gait conditions to serve as a benchmark for integrated energy harvesting management. This module is specifically designed to handle intermittent and high-impedance energy sources, providing a reference for comparison with discrete rectifier-based designs.

To ensure statistical rigor, each circuit configuration was tested in at least three independent walking trials at each treadmill speed. Results were averaged, and variability between trials was recorded to account for natural differences in gait. Only functional configurations were included in the final analysis.

## 2.3.4 Data acquisition and energy estimation

During treadmill walking trials, output voltages generated by the insole-embedded PZT plates were recorded using the FLUKE-287 true RMS digital multimeter (Fig. 10). Voltage readings were taken at the terminals of both the test capacitor (1000 µF, 16 V) and the lithiumion battery (Nokia BL-5B, 3.7 V, 890 mAh) before and after defined walking durations. The instrument's high accuracy ensured reliable comparison between trials, while repeated baseline checks confirmed the reproducibility of results. In this system, the piezoelectric plates act as self-powered sensors that detect plantar pressure variations. The mechanical strain generated during heel strike and push-off induces charge separation within the PZT ceramics, producing an alternating electrical signal. This AC voltage is extracted through lead wires, rectified to DC using bridge circuits, and then delivered to the capacitor or lithium-ion battery. The measured

voltage increments therefore directly reflect both the magnitude of induced strain and the effectiveness of the energy conversion process, enabling simultaneous sensing and power harvesting during gait. In this design, the PZT plates inherently function as self-powered sensors. The mechanical loading during heel strike and toe-off modulates the piezoelectric charge generation, allowing the electrical output signal to directly represent plantar-pressure variation without external power or separate sensing circuitry. Therefore, sensing and harvesting proceed simultaneously, and any change in foot—insole mechanical interaction is automatically detected and recorded through the harvested voltage output.

Charging performance was evaluated using two practical indicators:

- (1) Capacitor voltage increments the change in capacitor terminal voltage after each walking trial reflected the ability of different circuit configurations to capture and temporarily store energy under cyclic gait loading.
- (2) Battery voltage increments the increase in BL-5B battery terminal voltage after walking represented the feasibility of long-term charging in a realistic storage medium.

This voltage-based evaluation method reflects the actual scope of the experimental data collected in this study. By focusing on incremental changes at both capacitors and battery terminals, the assessment extended beyond simple open-circuit piezoelectric voltage readings and provided a reproducible basis for comparing circuit configurations under real-world gait conditions.

#### 3. Results

In this section, we present the experimental results obtained from the insole-embedded piezoelectric energy harvesting system. The analysis focuses on three primary factors: (i) the placement of piezoelectric plates under different plantar regions, (ii) the effect of rectifier circuit configurations including AC/DC and series/parallel arrangements, and (iii) the effect of walking speeds ranging from 3 to 5 km/h on charging performance. Both short-term storage behavior, represented by voltage increments across a test capacitor, and long-term charging feasibility, assessed through battery voltage increments of a BL-5B lithium-ion cell, were systematically evaluated.

To ensure clarity, the results are organized into subsections corresponding to each variable of interest. Tables and figures are employed to quantitatively summarize the observed voltage increments, while the accompanying text highlights key trends and performance differences. This structure allows the straightforward comparison of circuit topologies and gait conditions, thereby identifying the most effective configurations for wearable piezoelectric energy harvesting applications.

## 3.1 Effect of piezoelectric plate placement

To identify the optimal placement of piezoelectric elements within the insole, the plantar pressure distribution during walking was first examined. A foot pressure mapping experiment (Fig. 12) confirmed that the heel and metatarsal regions sustain the highest ground reaction forces, particularly during heel strike and push-off phases of the gait cycle. On the basis of this



Fig. 12. (Color online) Plantar pressure distribution and heel zone division. The heel was divided into a  $3 \times 3$  grid (zones 1-7) to identify high-pressure regions. The central zone (zone 5) corresponds to the anatomical heel center, which receives the highest ground reaction force during heel strike.

distribution, two types of PZT-5 ceramic plate were tested: Plate A ( $60 \text{ mm} \times 20 \text{ mm}$ ) positioned under the metatarsal region, and Plate B ( $40 \text{ mm} \times 20 \text{ mm}$ ), which was evaluated at seven distinct heel zones defined by a  $3 \times 3$  grid (zones 1–7).

Each zone was tested under identical conditions using a bridge rectifier circuit and capacitor storage. Table 3 shows the measured voltage increments across the seven heel zones. The results demonstrated notable spatial variation. The highest voltage output was recorded at zone 5 (5.7162 V), corresponding to the anatomical center of the heel. Zones 2 (4.3729 V) and 7 (5.3618 V) also yielded relatively high values, while the lowest performance was observed at zone 3 (2.8475 V). Intermediate results were obtained at zone 1 (3.5614 V), zone 4 (3.9205 V), and zone 6 (3.7389 V).

These results indicate that the central heel (zone 5) provides the most favorable loading condition for energy harvesting, with adjacent zones (2 and 7) also contributing effectively. In contrast, lateral regions such as zone 3 showed weaker performance, consistent with their reduced plantar pressure during gait.

Additional trials were conducted to evaluate the orientation of Plate A under vertical alignment at zones 2, 5, and 7. However, vertical placement led to excessive bending stress, causing cracks in the ceramic after several loading cycles. This outcome highlights that not only placement location but also orientation must be carefully considered to ensure both optimal energy harvesting and mechanical durability.

Although this study focused on a single participant, foot morphology (e.g., heel width, arch height) and shoe size can alter plantar-pressure distribution and shift strain hot spots. Such interindividual variability may change the optimal transducer placement and the amount of harvested energy. To ensure broader applicability, future work will recruit participants with diverse foot geometries and sizes and reevaluate the placement map and charging metrics under identical circuit settings.

Table 3 Voltage outputs of Plate B  $(40 \times 20 \text{ mm}^2)$  at seven heel zones during 1 min of treadmill walking at 3 km/h. Results indicate that the central heel (zone 5) provided the highest output, while peripheral regions showed comparatively lower performance.

Zone	Voltage (V)	
1	3.3296	
2	4.3729	
3	3.2376	
4	3.9297	
5	5.7162	
6	3.7835	
7	5.3618	

# 3.2 Effect of different bridge rectifier configurations

The charging performance of piezoelectric energy harvesting systems is strongly dependent on circuit topology. To examine this dependence, two complementary experiments were conducted.

First, a cantilever-based setup was employed (Fig. 13) to provide a controlled and repeatable test platform. In this configuration, a PZT-5 piezoelectric plate was fixed to a cantilever beam, and a permanent magnet was attached to its free end. A facing electromagnet generated alternating repulsive magnetic forces, causing the cantilever to vibrate periodically. This vibration induced strain in the piezoelectric plate, generating alternating voltage that was subsequently rectified and stored in a capacitor. The four tested bridge rectifier configurations (AC series, AC parallel, DC series, and DC parallel) produced distinctly different voltage outcomes (Table 4). The AC parallel and DC parallel configurations achieved significantly higher capacitor voltages (6.3518 and 6.4219 V) than their series counterparts (2.1372 and 1.8762 V), confirming that parallel connections transfer energy more efficiently under dynamic excitation.

Second, insole-based experiments were conducted to replicate realistic gait-induced loading. A 70 kg participant alternated slow left–right single-foot standing, producing repeatable heel strikes while minimizing gait variability. Each circuit configuration was tested in five separate trials, and average capacitor voltages were calculated (Table 5). Results again demonstrated the superiority of parallel configurations. The AC parallel and DC parallel topologies reached mean voltages of 3.6958 and 3.7991 V, whereas the AC series and DC series configurations yielded much lower values of 2.2926 and 2.1006 V, respectively. Importantly, the parallel topologies not only provided higher voltage outputs but also exhibited smaller trial-to-trial variation (<0.02 V), whereas the series configurations showed greater variability.

Together, these findings confirm that parallel strategies—particularly the DC parallel connection—are the most effective and stable for charging capacitors under both controlled and gait-based conditions. Consequently, subsequent analyses of walking speed effects focused on four representative cases: a single piezoelectric plate, the two most efficient topologies (AC parallel and DC parallel), and a commercial EH301A module as a benchmark.

A clear hierarchy was observed: DC parallel > AC parallel » AC series > DC series. This confirms that parallel architectures ensure that each plate contributes independent current, while series structures suffer from intermittent mechanical inactivity during gait.

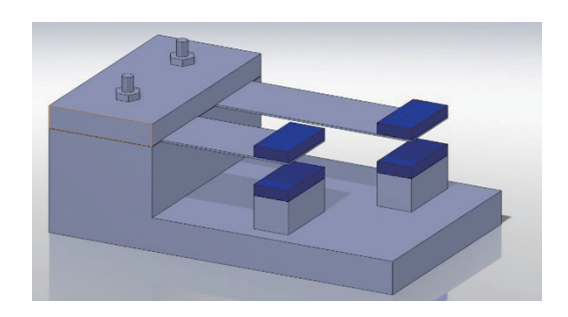


Fig. 13. (Color online) Cantilever-based experimental setup for testing piezoelectric bridge rectifier configurations.

Table 4 Capacitor charging performance of four bridge rectifier configurations under cantilever excitation (mean  $\pm$  SD, N = 3).

Configuration	Avg. max voltage (V)	Relative performance
AC sries	$2.14 \pm 0.01$	baseline
DC series	$1.88 \pm 0.02$	-12% vs AC-S
AC parallel	$6.35 \pm 0.03$	+197% vs AC-S
DC parallel	$6.42\pm0.02$	+200% vs AC-S

Table 5 Capacitor charging performance during alternating single-foot standing ( $mean \pm SD$ , five trials).

Configuration	Avg. max voltage (V)	Stability (SD)	Performance ranking
AC series	$2.29 \pm 0.01$	Moderate	4
DC series	$2.10\pm0.01$	Moderate	3
AC parallel	$3.70\pm0.01$	High	2
DC parallel	$3.80 \pm 0.01$	High	1

## 3.3 Effect of walking speed

Experimental evaluation was conducted to assess the energy harvesting performance of piezoelectric systems integrated into footwear under real walking conditions. Multiple circuit configurations were examined to quantify their effectiveness in charging a lithium battery at different walking speeds (3, 4, and 5 km/h). The investigation focused on comparing voltage increments resulting from sustained gait-induced mechanical excitation, providing a detailed analysis of how circuit topology affects the overall energy conversion efficiency. Each trial comprised three consecutive 20 min walking sessions, with cumulative voltage rise recorded to evaluate practical energy harvesting potential under realistic usage scenarios.

# 3.3.1 Single piezoelectric plate

Piezoelectric Plate B was positioned at the optimal heel zone (zone 5), which was previously identified as the area with the highest plantar pressure based on foot pressure distribution analysis. This zone experiences peak compressive forces during the heel-strike phase of the gait cycle, making it a prime candidate for energy harvesting. Walking experiments at three speeds—3, 4, and 5 km/h—were performed to examine how kinetic parameters affect charging performance. As summarized in Tables 6–8, cumulative battery voltage increases of 0.0222, 0.0266, and 0.0304 V were recorded, respectively.

Table 6
Experimental results with a single piezoelectric plate (3 km/h walking speed for 20 min and total distance of 1.0 km).

77.1.	No.		
Voltage	1	2	3
Initial voltage	3.7537 V	3.7609 V	3.7692 V
Stable average voltage	3.7609 V	3.7692 V	3.7759 V
Difference	0.0072 V	0.0083 V	0.0067 V
Total voltage rise		0.0222 V	

Table 7
Experimental results with a single piezoelectric plate (4 km/h walking speed continues 20 min; total distance 1.3 km).

77-14	No.		
Voltage	1	2	3
Initial voltage	3.7608 V	3.7609 V	3.7692 V
Stable average voltage	3.7680 V	3.7692 V	3.7759 V
Difference	0.0072 V	0.0083 V	0.0067 V
Total voltage rise		0.0266 V	

Table 8
Experimental results with a single piezoelectric plate (5 km/h walking speed continues 20 min; total distance 1.6 km).

37.14	No.		
Voltage	1	2	3
Initial voltage	3.7724 V	3.7609 V	3.7692 V
Stable average voltage	3.7829 V	3.7692 V	3.7759 V
Difference	0.0105 V	0.0083 V	0.0067 V
Total voltage rise		0.0304 V	

The data reveal a clear trend of enhanced energy harvesting efficiency with increasing walking speed. This outcome can be attributed to two key biomechanical factors: (1) a higher cadence at higher speeds results in a more frequent mechanical loading of the piezoelectric plate, effectively increasing the duty cycle of energy input; and (2) greater impact force during each footfall amplifies the mechanical strain applied to the transducer, leading to larger electrical outputs per cycle. Notably, even with a single piezoelectric plate, the system demonstrated measurable voltage increments, highlighting the feasibility of low-profile, single-module harvesting setups for ultralow-power wearable electronics.

However, the voltage rise remained modest, emphasizing that while a single module can supplement energy needs, its standalone contribution is limited without circuit enhancements or additional transducer elements.

## 3.3.2 AC parallel circuit

Piezoelectric Plate A (installed under the metatarsal) and Plate B (heel, zone 5) were connected using the AC parallel configuration. The cumulative battery voltage rises were measured as 0.0463, 0.0533, and 0.0644 V at walking speeds of 3, 4, and 5 km/h, respectively

(Tables 9–11). This configuration yielded nearly double the output compared with the single-plate setup across all speeds, underscoring the effectiveness of parallel connection in amplifying total harvested energy.

The AC parallel topology operates by connecting the AC outputs of multiple piezoelectric plates directly in parallel before rectification. Since each piezoelectric transducer generates an alternating voltage when subjected to mechanical stress, their combined effect in the parallel connection effectively sums the individual currents, while the output voltage remains capped at the level of the highest-performing plate. This design principle ensures that while the open-circuit voltage of each plate is not additive, the cumulative current is, which is critical for applications where the capacitor charging rate is governed primarily by available current.

The observed increase in charging performance with walking speed reflects the synergistic action of the two transducers under dynamic loading. Higher speeds result in more frequent mechanical excitation cycles, and the combined foot pressure at both the heel and metatarsal regions contributes to a greater simultaneous mechanical deformation of both plates. This results in overlapping AC current peaks, thereby reinforcing the net current output into the rectifier. Additionally, the mechanical phase offset between the heel strike and forefoot push-off phases of gait creates a form of natural current smoothing, which benefits the overall energy harvesting efficiency by reducing periods of inactivity in the output waveform.

Table 9 Experimental results with AC parallel circuit (3 km/h walking speed continues 20 min; total distance 1.0 km).

T7 14	No.		
Voltage	1	2	3
Initial voltage	3.8042 V	3.8184 V	3.8347 V
Stable average voltage	3.8184 V	3.8347 V	3.8505 V
Difference	0.0142 V	0.0163 V	0.0158 V
Total voltage rise		0.0463 V	

Table 10 Experimental results with AC parallel circuit (4 km/h walking speed continues 20 min; total distance 1.3 km).

Voltage	No.		
	1	2	3
Initial voltage	3.6783 V	3.6955 V	3.7141 V
Stable average voltage	3.6955 V	3.7141 V	3.7316 V
Difference	0.0172 V	0.0186 V	0.0175 V
Total voltage rise		0.0533 V	

Experimental results with AC parallel circuit (5 km/h walking speed continues 20 min; total distance 1.6 km).

V-14	No.		
Voltage	1	2	3
Initial voltage	3.7635 V	3.7838 V	3.8054 V
Stable average voltage	3.7838 V	3.8054 V	3.8279 V
Difference	0.0203 V	0.0216 V	0.0225 V
Total voltage rise		0.0644 V	

One key observation is that although AC parallel configurations are straightforward and costeffective, they can suffer from phase mismatch or destructive interference if the connected
piezoelectric plates generate out-of-phase voltages owing to differences in mechanical loading
timing. In this experiment, the placement of plates in distinct gait zones—heel and metatarsal—
introduces a predictable temporal offset between their activation peaks. While this did not cause
notable adverse effects in the current setup, future designs incorporating more than two plates or
plates in asynchronous positions may require additional circuit considerations, such as isolation
diodes or individual rectification paths, to prevent potential backflow currents or losses.

Overall, the AC parallel configuration demonstrated substantial improvements in current output and charging speed, validating its applicability for multisource wearable energy harvesting systems, especially where simplicity and low-cost integration are prioritized.

# 3.3.3 DC parallel circuit

The same piezoelectric plate arrangement was evaluated using the DC parallel configuration, where each plate was connected to its own bridge rectifier and subsequently combined at the DC side. The cumulative battery voltage increases were recorded as 0.0503, 0.0607, and 0.0733 at 3, 4, and 5 km/h, respectively (Tables 12–14). These results surpassed the AC parallel configuration by a modest yet consistent margin across all test speeds.

Table 12 Experimental results with DC parallel circuit (3 km/h walking speed continues 20 min; total distance 1.0 km).

Voltage	No.		
	1	2	3
Initial voltage	3.8062 V	3.8184 V	3.8347 V
Stable average voltage	3.8225 V	3.8347 V	3.8505 V
Difference	0.0163 V	0.0163 V	0.0158 V
Total voltage rise		0.0503 V	

Table 13 Experimental results with DC parallel circuit (4 km/h walking speed continues 20 min; total distance 1.3 km).

Voltage	No.		
	1	2	3
Initial voltage	3.7965 V	3.8163 V	3.8368 V
Stable average voltage	3.8163 V	3.8368 V	3.8572 V
Difference	0.0198 V	0.0205 V	0.0204 V
Total voltage rise		0.0607 V	

Experimental results with DC parallel circuit (5 km/h walking speed continues 20 min; total distance 1.6 km).

Voltage	No.		
	1	2	3
Initial voltage	3.7835 V	3.7838 V	3.8054 V
Stable average voltage	3.8068 V	3.8054 V	3.8279 V
Difference	0.0233 V	0.0216 V	0.0225 V
Total voltage rise		0.0733 V	

The superior performance of the DC parallel setup can be attributed to its structural advantage in handling asynchronous mechanical excitation. Each piezoelectric plate operates as an independent power-generating unit, converting mechanical energy into rectified DC output through its own rectification path. This separation ensures that any phase differences arising from the gait cycle—such as the natural time lag between heel strike and forefoot push-off—do not result in destructive interference or current cancellation, which is a known issue in AC parallel systems. Instead, even when one plate is inactive or produces minimal output (e.g., during mid-stance or swing phases), the other plate continues to deliver rectified DC current to the storage capacitor without interruption.

Another technical advantage lies in reducing parasitic losses. In AC parallel configurations, the simultaneous operation of multiple transducers can introduce back-current effects or voltage reversal issues, especially if the mechanical input is uneven. The DC parallel approach circumvents this by isolating each transducer's rectification stage, thereby eliminating the risk of mutual interference and ensuring unidirectional current flow at the DC bus. This architecture not only enhances output stability but also extends system longevity by reducing electrical stress on components.

The data also highlight that as walking speed increases, the benefit of DC parallel architecture becomes even more pronounced. At 5 km/h, the voltage gain was 0.0733 V—about 45% higher than that of the single-plate setup and slightly exceeding that of the AC parallel circuit. This suggests that the DC parallel configuration scales effectively with increased mechanical excitation, making it particularly suitable for applications where variable gait patterns are expected, such as during jogging or brisk walking.

However, note that while the DC parallel circuit improves consistency and efficiency, it introduces greater circuit complexity and increases the component count (requiring one rectifier per piezoelectric plate). This can slightly raise the overall cost and footprint of the system. For large-scale arrays with many transducers, future work can explore optimized rectification strategies such as hybrid partial-rectifier sharing or integrated power management ICs to balance performance and complexity.

In summary, the DC parallel configuration offers enhanced robustness and superior energy conversion performance, especially in dynamic, real-world scenarios where mechanical excitation is not perfectly synchronized across transducers. This makes it a highly promising architecture for wearable piezoelectric energy harvesting systems aiming for reliable operation under variable conditions.

## 3.3.4 EH301A module

The EH301A module was evaluated under the same walking conditions as other configurations, using the same piezoelectric plate arrangement (Plate A under the metatarsal and Plate B at heel zone 5). The cumulative battery voltage increments were measured at 0.0394, 0.0437, and 0.0500 V for walking speeds of 3, 4, and 5 km/h, respectively (Tables 15–17). Although these results were slightly lower than those observed for the DC and AC parallel circuits, the EH301A module demonstrated consistent and reliable performance throughout all test cycles.

Table 15 Experimental results with EH301A module (3 km/h walking speed continues 20 min; total distance 1.0 km).

Voltage	No.		
	1	2	3
Initial voltage	3.7608 V	3.7735 V	3.7866 V
Stable average voltage	3.7735 V	3.7866 V	3.8002 V
Difference	0.0127 V	0.0131 V	0.0136 V
Total voltage rise		0.0394 V	

Table 16 Experimental results with EH301A module (4 km/h walking speed continues 20 min; total distance 1.3 km).

Voltage	No.		
	1	2	3
Initial voltage	3.7852 V	3.7998 V	3.8133 V
Stable average voltage	3.7998 V	3.8133 V	3.8289 V
Difference	0.0146 V	0.0135 V	0.0156 V
Total voltage rise		0.0437 V	

Table 17 Experimental results with EH301A module (5 km/h walking speed continues 20 min; total distance 1.6 km).

Voltage	No.		
	1	2	3
Initial voltage	3.8125 V	3.8290 V	3.8453 V
Stable average voltage	3.8290 V	3.8453 V	3.8625 V
Difference	0.0165 V	0.0163 V	0.0172 V
Total voltage rise		0.0500 V	

EH301A is a specialized energy harvesting power management module engineered to handle unstable, high-impedance energy sources such as piezoelectric transducers. Its internal architecture includes a proprietary energy capture and release mechanism based on voltage threshold detection: once the internal capacitor reaches the high threshold voltage (VH = 5.2 V), the module activates its output stage, delivering accumulated energy to the battery. Discharging continues until the voltage drops to a lower threshold (VL = 3.1 V), at which point the circuit automatically halts output to begin a new charging cycle. This hysteresis-based control ensures that energy is only delivered in efficient, usable bursts, avoiding the inefficiencies of continuous low-current trickle charging.

One of the most notable observations during testing was the module's ability to maintain stable charging cycles even under intermittent mechanical input. Unlike passive rectifier circuits, which directly transfer a fluctuating piezoelectric output to the battery (resulting in highly variable charging current), the EH301A module's internal buffer capacitor smooths out these fluctuations. This buffering effect led to a remarkably consistent charging pattern, with minimal voltage ripple observed across cycles, even when footstep impacts were irregular.

However, while the module's smart regulation contributed to enhanced operational stability and safety, it also introduced inherent trade-offs. First, the EH301A module requires a minimum energy threshold before it can trigger the output phase, meaning that small amounts of harvested energy may be stored for extended periods without immediate contribution to battery charging. This explains the slightly lower net voltage rise observed than those obtained with the DC and AC parallel circuits, where every increment of generated current—no matter how small—was

instantly delivered to the battery. Compared with popular energy-harvesting ICs such as LTC3588-1 (Analog Devices), which provides efficient AC-to-DC conversion but requires a minimum input level to activate, and SPV1050 (STMicroelectronics), which enables MPPT-based optimization but increases complexity and quiescent power consumption, the EH301A module offers a practical balance between efficiency, reliability, and simplicity. These characteristics support its suitability for highly intermittent piezoelectric outputs during human gait.

Additionally, the module's sophisticated energy management circuitry incurs its own overhead losses. The energy required to operate internal monitoring, threshold detection, and control logic consumes part of the harvested energy, which further reduces the net charging efficiency. Measurements showed that during initial stages of walking, especially at lower speeds (3 km/h), there were notable delays before the module's output phase activated, reflecting the time needed to build up sufficient internal charge.

From a system design perspective, these trade-offs are acceptable or even beneficial in many real-world scenarios where reliability, battery safety, and consistent output are prioritized over raw harvesting efficiency. For example, in medical wearables or critical sensor systems, the EH301A module's protective mechanisms prevent overcharging and unstable voltage conditions that can damage sensitive components or compromise user safety.

Looking ahead, potential optimizations can include adjusting the hysteresis window (VH and VL thresholds) to better align with the specific voltage profile of the piezoelectric source and battery characteristics. Additionally, integrating ultralow-power monitoring circuits or adaptive energy gating can further reduce internal overhead and improve net efficiency, especially at lower activity levels.

In summary, while the EH301A module's peak energy harvesting performance was modestly lower than that of passive DC parallel configurations, it delivered superior regulation, safety, and operational robustness. These attributes highlight its strong suitability for wearable applications where reliable energy management is as critical as maximizing harvesting efficiency.

Across all circuit configurations, increasing walking speed from 3 to 5 km·h<sup>-1</sup> consistently improved cumulative battery voltage rise. This trend is explained by two biomechanical factors: higher cadence, which increases the number of excitation cycles per unit time, and larger heelstrike force, which amplify per-cycle strain, both of which elevate net charge transfer. Notably, the performance ranking remained unchanged (DC-parallel > AC-parallel > EH301A > single plate), indicating that circuit topology—not speed alone—dominates usable energy gain under gait.

## 3.3.5 Performance comparison of various circuit configurations

Figure 14 presents a comparative summary of the battery voltage rise achieved under different circuit configurations across three walking speeds (3, 4, and 5 km/h). The DC parallel circuit consistently outperformed other setups, achieving the highest energy conversion efficiency at all test speeds. Specifically, at 5 km/h, the DC parallel configuration recorded a cumulative battery voltage increase of approximately 0.0733 V, surpassing both the AC parallel circuit (~0.0644 V) and the EH301A module (~0.0500 V).

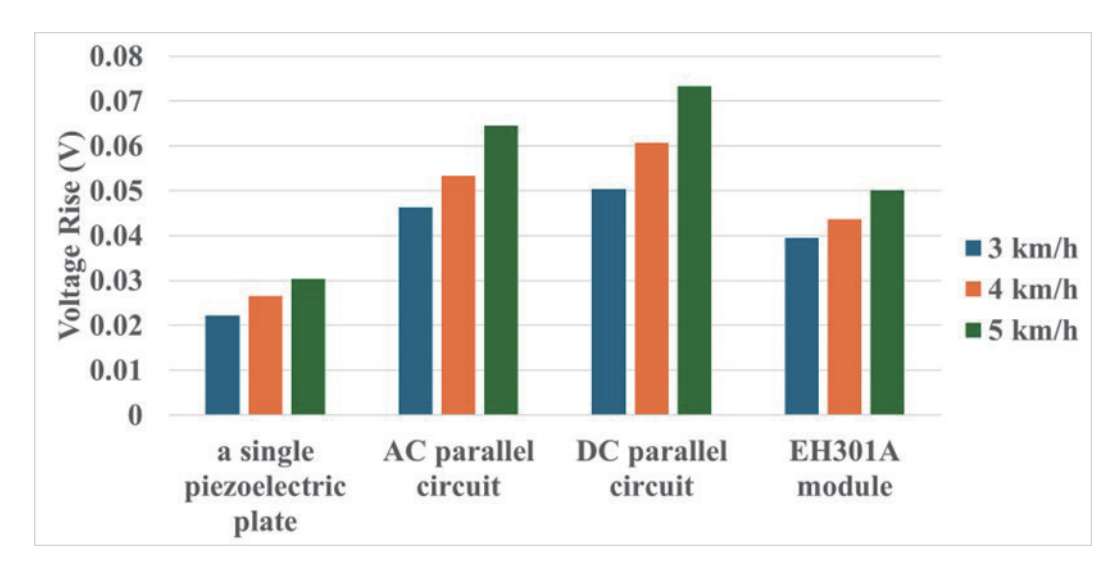


Fig. 14. (Color online) Comparison of battery voltage rise under different circuit configurations and walking speeds.

The superior performance of DC parallel architecture can be attributed to its intrinsic ability to handle asynchronous mechanical inputs efficiently. By ensuring that each piezoelectric plate rectifies its output independently before contributing to the DC bus, the system minimizes phase interference and allows for maximized cumulative energy capture. This was particularly evident at higher walking speeds, where foot impact events are more frequent, and the DC parallel configuration was able to scale its performance effectively.

The AC parallel circuit, while slightly less efficient, still demonstrated significant gains over the single-plate configuration. Its advantage lies in the simplicity of its circuit design and reduced component count, making it an attractive option when system compactness and cost are critical considerations.

The EH301A module, although trailing in raw energy harvesting efficiency, excelled in output stability and safety. Its regulated output cycles ensured smooth and controlled charging, making it particularly suited for applications where power consistency is paramount—such as medical wearables or precision monitoring devices.

Note that repeated mechanical loading led to instances of piezoelectric ceramic layer delamination and fracturing, particularly under the high-pressure zones (heel area). This mechanical degradation limited the long-term durability of the system. To mitigate these issues, piezoelectric plates were coated with a layer of hot-melt adhesive to reinforce their mechanical integrity. While this approach improved resistance to cracking and enhanced overall robustness, partial plate failures were still occasionally observed, indicating that further material optimization—such as employing flexible piezoelectric composites or multi-layered encapsulation—may be necessary for prolonged field deployment.

In summary, the DC parallel circuit offers the highest raw energy harvesting performance, the AC parallel circuit provides good balance between efficiency and simplicity, and the EH301A module prioritizes operational stability and safety. These findings highlight the importance of tailoring energy harvesting circuit architectures to the specific application context, balancing performance, reliability, and complexity.

## 4. Discussion

In this study, we systematically examined the effects of piezoelectric plate placement, circuit configuration, and gait speed on the performance of a wearable insole-based energy harvesting system. The results highlight several key insights relevant to the design of practical energy harvesting footwear.

The heel and metatarsal regions were confirmed as optimal zones for embedding piezoelectric plates owing to their high plantar pressures during heel strike and push-off. Plate B positioned at the heel center (zone 5) consistently yielded the highest output voltage, reflecting the strong compressive forces experienced at this site. Vertical orientations were shown to be mechanically unstable, often causing premature ceramic fracture, which underlines the necessity of aligning plate geometry with natural foot mechanics. These findings align with those of Paradiso and Starner, who also emphasized that the non-optimized placement and orientation of piezoelectric devices significantly limit achievable energy density in footwear applications. Furthermore, the effectiveness of piezoelectric energy harvesting is strongly affected by biomechanical variability during gait. Higher ground reaction forces increase strain input, while phase delays between different plantar regions require circuit architectures capable of preventing destructive interference. Efficient impedance matching is also essential to minimize energy loss across diodes and capacitors, ensuring maximum charge extraction during each footfall. Collectively, these mechanical–electrical coupling parameters constitute the dominant sensitivity factors governing real-world harvesting efficiency.

A critical finding of this work is the superior performance of parallel configurations (both AC and DC) over their series counterparts. Although electrical theory suggests that series connections should increase voltage, experimental data demonstrated the opposite: AC series and DC series circuits produced significantly lower capacitor voltages than AC parallel and DC parallel designs. The underlying reason is rooted in the asynchronous and intermittent nature of gait-induced excitation. When one piezoelectric element is inactive, it effectively behaves as a resistive load, suppressing net output voltage. In contrast, parallel configurations allow active elements to contribute current independently, while inactive ones do not hinder delivery. This explains the higher and more stable charging performance of parallel circuits under real walking conditions. Li *et al.* (2018)<sup>(13)</sup> similarly reported that the parallel connection of piezoelectric modules achieved higher power densities (~1.5 mW/cm²), supporting our observation that parallel circuits—especially in DC mode—are more effective in enhancing current output under low-frequency gait excitation.

The DC parallel configuration, in particular, demonstrated the most consistent performance, as each plate was rectified individually before combining at the DC bus. This architecture mitigates destructive interference caused by asynchronous mechanical inputs and ensures unidirectional current flow. While this increases component count, the efficiency gain is crucial for real-world wearable systems.

Wearable piezoelectric harvesting platforms have predominantly utilized flexible PVDF-based transducers owing to their mechanical adaptability and biocompatibility under low-curvature motions. (14,15) However, most insole studies emphasized plantar pressure sensing rather than optimizing electrical energy output across high-pressure gait regions. By integrating

the heel-forefoot placement strategy with circuit optimization, our work addresses both spatial and electrical constraints simultaneously.

Furthermore, conventional full-bridge rectifiers suffer from destructive interference when asynchronous excitations occur between the heel and forefoot. Our results demonstrate that DC parallel architecture mitigates this issue and achieves more stable charge accumulation, which aligns with prior findings on advanced rectifiers such as sense-and-set (SaS) and SSHI-enhanced circuits that significantly boost power extraction efficiency. (16,17)

In addition, unlike previous systems that lacked power conditioning capability, our implementation of the EH301A module reduces voltage fluctuation throughout the gait cycle. This is consistent with recent reviews that highlight the substantial enhancement of harvesting reliability in batteryless wearable applications by integrating MPPT and cold-start-enabled power interfaces.<sup>(18)</sup>

These improvements collectively demonstrate that the proposed integration strategy offers a more robust and practical energy harvesting performance than earlier insole-based designs.

The EH301A module provided the most stable and regulated charging behavior, effectively buffering intermittent piezoelectric output. Specifically, the EH301A module employs hysteretic charge control with  $VH \approx 5.2$  V and  $VL \approx 3.1$  V, releasing buffered energy in bursts once the upper threshold is reached. For context, benchmark ICs such as LTC3588-1 (Analog Devices) and SPV1050 (STMicroelectronics) offer efficient AC-to-DC conversion and MPPT/cold-start capabilities, respectively, but at the cost of increased complexity and quiescent power. A head-to-head hardware comparison is planned in future work. However, this stability came at the cost of reduced immediate energy conversion efficiency, reflecting the trade-off between output robustness and raw performance. Fan *et al.*<sup>(19)</sup> highlighted similar trade-offs in active energy management circuits, which improve long-term safety and reliability but reduce instantaneous conversion efficiency. Thus, application context determines the preferable architecture: DC parallel for maximizing harvested energy or EH301A-like modules for regulated and safe power delivery in sensitive devices.

Results further showed that increasing walking speed led to greater cumulative battery voltage rise across all circuit configurations. This is attributed to both the higher cadence (more frequent loading cycles) and greater impact forces at higher speeds, which enhance mechanical-to-electrical energy conversion. The relative ranking of circuit performance (DC parallel > AC parallel > EH301A > single plate) remained consistent across speeds, confirming robustness. This indicates that while speed elevates the absolute harvested energy through cadence and impact, the circuit topology remains the dominant determinant of usable charge under gait. Similar trends of speed-dependent efficiency have been described in prior biomechanical harvester studies.<sup>(12)</sup>

Repeated loading resulted in the occasional delamination and fracture of PZT plates, even after reinforcement with hot-melt adhesive. Additionally, foot geometry including arch height, heel width, and forefoot curvature affects local plantar pressure distribution and thus the strain applied to piezoelectric plates. To ensure broader applicability, future work will recruit participants with diverse foot sizes and morphologies and re-evaluate the placement map and charging metrics under identical circuit settings. Since this study involved a single footwear size

and participant profile, inter-individual variability could not be fully characterized. Future work will recruit participants with different foot shapes and sizes to ensure broader biomechanical applicability. This corroborates the observations of Wu *et al.*,<sup>(20)</sup> who reported the brittleness of PZT ceramics in wearable contexts. Their findings, together with ours, emphasize the growing need to adopt flexible polymer-based piezoelectric materials (e.g., PVDF composites) to balance efficiency with long-term mechanical resilience.

Overall, this study demonstrates that effective energy harvesting from gait requires integrated optimization of biomechanical placement, circuit architecture, and gait conditions. Parallel circuit topologies—particularly DC parallel—overcome the limitations of series connections under intermittent loading. Meanwhile, commercial modules such as EH301A ensure stable and safe operation at the expense of peak efficiency. By comparing these strategies under realistic walking conditions, the present work extends prior literature and provides new insights for designing practical, low-power wearable energy harvesting systems. In practice, we recommend DC parallel as the default topology for footwear harvesters subject to asynchronous heelforefoot loading and an EH301A-class interface when regulated delivery and battery safety outweigh peak efficiency.

#### 5. Conclusion

In this study, we developed and systematically evaluated a piezoelectric energy harvesting system embedded in a shoe insole for wearable power applications. The investigation confirmed that a careful optimization of plate placement, circuit configuration, and gait conditions is essential for maximizing harvesting efficiency. Placement analysis identified the heel center (zone 5) and metatarsal region as the most effective locations for piezoelectric transducers, corresponding to peak plantar pressures during walking.

Circuit topology comparisons revealed that parallel connections—particularly the DC parallel configuration—achieved a significantly higher charging performance than series connections. The reduced efficiency of series circuits was attributed to inactive elements behaving as resistive loads under intermittent gait excitation, suppressing net output voltage. In contrast, parallel circuits enabled active elements to deliver current independently, ensuring greater stability and higher cumulative energy capture.

Walking trials at 3, 4, and 5 km/h further demonstrated that increased gait speed enhanced energy harvesting efficiency owing to higher cadence and impact forces. Among the tested architectures, the DC parallel circuit achieved the greatest voltage rise, followed by the AC parallel configuration. The EH301A module, while less efficient in raw energy transfer, exhibited superior regulation and output stability, highlighting the trade-off between peak performance and operational robustness.

Despite these promising results, the durability of PZT ceramics under repeated loading remains a limitation, as mechanical delamination and fracture were observed. Future research should focus on exploring flexible piezoelectric composites, advanced encapsulation strategies, and integrated power management solutions to enhance both mechanical resilience and overall energy conversion efficiency.

In summary, this work contributes a systematic comparison of circuit architectures under realistic walking conditions, providing new insights into the design of wearable piezoelectric energy harvesting systems. The findings underscore the importance of tailoring device architecture to balance efficiency, reliability, and durability, advancing the potential of self-powered wearable electronics. Furthermore, the proposed system functions as a pressure-driven self-powered sensor that simultaneously detects plantar-force-induced strain and converts it into regulated electrical energy. The electrical output therefore serves as a direct physiological indicator of gait dynamics while also powering low-energy wearable electronics. These findings reinforce the practical pathway toward scalable, sensing-enabled, self-sustained healthmonitoring systems and smart IoT footwear applications.

#### References

- 1 R. M. Dell and D. A. J. Rand: J. power sources 100 (2001) 2. https://doi.org/10.1016/S0378-7753(01)00894-1
- 2 IEA: World energy outlook 2022 (IEA, Paris, 2022). https://www.iea.org/reports/world-energy-outlook-2022
- 3 S. Priya, H.-C. Song, Y. Zhou, R. Varghese, A. Chopra, S.-G. Kim, I. Kanno, L. Wu, D. S. Ha, and J. Ryu: Energy harvesting Syst. 4 (2019) 3. <a href="https://doi.org/10.1515/ehs-2016-0028">https://doi.org/10.1515/ehs-2016-0028</a>
- 4 S. Roundy, P. K. Wright, and J. Rabaey: Comput. Commun. **26** (2003) 1131. <a href="https://doi.org/10.1016/S0140-3664(02)00248-7">https://doi.org/10.1016/S0140-3664(02)00248-7</a>
- 5 H. Li, C. Tian, and Z. D. Deng: Appl. Phys. Rev. 1 (2014) 041301. https://doi.org/10.1063/1.4900845
- 6 C. B. Williams and R. B. Yates: Sens. Actuators, A 52 (1996) 8. https://doi.org/10.1016/0924-4247(96)80118-X
- 7 E. O. Torres and G. A. Rincón-Mora: J. Energy Eng. 134 (2008) 121. <a href="https://doi.org/10.1061/(ASCE)0733-9402(2008)134:4(121)">https://doi.org/10.1061/(ASCE)0733-9402(2008)134:4(121)</a>
- 8 S. Priya and D. J. Inman: Energy Harvesting Technologies (Springer, 2009) Vol. 21, <a href="https://doi.org/10.1007/978-0-387-76464-1">https://doi.org/10.1007/978-0-387-76464-1</a>
- 9 K. Uchino: Piezoelectric Actuators and Ultrasonic Motors (Springer Science & Business Media, 1996) Vol. 1, https://doi.org/110.1007/978-1-4613-1463-9
- 10 B. Zhao, F. Qian, A. Hatfield, L. Zuo, and T.-B. Xu: Sensors 23 (2023) 5841. https://doi.org/10.3390/s23135841
- 11 L. Liu, X. Guo, W. Liu, and C. Lee: Nanomaterials 11 (2021) 2975. https://doi.org/10.3390/nano11112975
- 12 J. A. Paradiso and T. Starner: IEEE Pervasive Comput. 4 (2005) 18. https://doi.org/10.1109/MPRV.2005.9
- 13 Z. Li, M. Zhu, Q. Qiu, J. Yu, and B. Ding: Nano Energy 53 (2018) 726. <a href="https://doi.org/10.1016/j.nanoen.2018.09.039">https://doi.org/10.1016/j.nanoen.2018.09.039</a>
- 14 S. Sukumaran, S. Chatbouri, D. Rouxel, E. Tisserand, F. Thiebaud, and T. Ben Zineb: J. Intell. Mater. Syst. Struct. **32** (2021) 746. <a href="https://doi.org/10.1177/1045389x20966058">https://doi.org/10.1177/1045389x20966058</a>
- 15 E. Iranmanesh, A. Rasheed, W. Li, and K. Wang: IEEE Trans. Electron Devices **65** (2018) 542. <a href="https://doi.org/10.1109/TED.2017.2780261">https://doi.org/10.1109/TED.2017.2780261</a>
- 16 Y. Peng, K. D. Choo, S. Oh, I. Lee, T. Jang, Y. Kim, J. Lim, D. Blaauw, and D. Sylvester: IEEE J. Solid-State Circuits 54 (2019) 3348. https://doi.org/10.1109/JSSC.2019.2945262
- 17 D. A. Sanchez, J. Leicht, F. Hagedorn, E. Jodka, E. Fazel, and Y. Manoli: IEEE J. Solid-State Circuits **51** (2016) 2867. <a href="https://doi.org/10.1109/JSSC.2016.2615008">https://doi.org/10.1109/JSSC.2016.2615008</a>
- 18 N. Almarri, J. Chang, W. Song, D. Jiang, and A. Demosthenous: Nano Energy 131 (2024) 110196. <a href="https://doi.org/10.1016/j.nanoen.2024.110196">https://doi.org/10.1016/j.nanoen.2024.110196</a>
- 19 F.-R. Fan, Z.-Q. Tian, and Z. L. Wang: Nano Energy 1 (2012) 328. <a href="https://doi.org/10.1016/j.nanoen.2012.01.004">https://doi.org/10.1016/j.nanoen.2012.01.004</a>
- 20 Q. Wu, H. Guo, H. Sun, X. Liu, H. Sui, and F. Wang: Ceramics Int. 47 (2021) 19614. <a href="https://doi.org/10.1016/j.ceramint.2021.03.299">https://doi.org/10.1016/j.ceramint.2021.03.299</a>

## **About the Authors**

Shang-Kuo Yang received the B.S. in 1982 and the M.S. in 1985 in Automatic Control Engineering from Feng Chia University, and the Ph.D. in 1999 in Mechanical Engineering from National Chiao Tung University, Taiwan, respectively. From 1985 to 1991, he was an assistant researcher and an instrumentation system engineer of the Flight Test Group, Aeronautic Research Laboratory, Zhong Shan Institute of Science and Technology, Taiwan. From 1991, he has been with the department of Mechanical Engineering at National Chin Yi University of Technology, Taiwan. His research interests are in reliability engineering, data acquisition system, biomedical engineering (cardiac pacemaker, patient nursing monitoring, otoliths restoration, drunk-driving prevention), and automation. (skyang@ncut.edu.tw)

**Po-Yang Shih** received his M.S. degrees from the National Chin Yi University of Technology, Taiwan, in 2013. His research interests are in MEMS, piezoelectric engineering, and sensors. (poyangshih@ncut.edu.tw)

Kai-Jung Chen is an accomplished individual with a Bachelor's degree in Engineering (2010), a Master's degree in Biomechanical Engineering (2012) from National Cheng Kung University in Taiwan, and a Ph.D. in Engineering from the University of Liverpool, UK (2019). During 2014-2019, he played a pivotal role in the Biomechanical Engineering Group at the University of Liverpool, focusing on precision ophthalmic equipment development. Currently, Kai-Jung is a faculty member in the Department of Mechanical Engineering at the National Chin-Yi University of Technology, Taiwan, since 2020. His diverse research interests include computational biomechanics, medical assistive device development, big data and AI technology, and semiconductor and brittle material processing. (hskchen5@ncut.edu.tw)